SAMSO TR-76-102

AN INVESTIGATION OF NOSE BLUNTNESS EFFECTS ON TRANSITION ASYMMETRY AND TRANSITION AERODYNAMICS

FINAL REPORT FOR PERIOD
1 MAY 1976 to 30 SEPTEMBER 1976
Contract No. F04701-75-C-0163

30 SEPTEMBER 1976

Prepared for:

HEADQUARTERS
SPACE AND MISSILE SYSTEMS ORGANIZATION
AIR FORCE SYSTEMS COMMAND
P. O. Box 92960
Worldway Postal Center
Los Angeles, California 90009

APPROVED FOR PUBLIC RELEASE; DISTRIBUTION UNLIMITED

TRW
DEFENSE AND SPACE SYSTEMS GROUP

One Space Park
Redondo Beach, California 90278

This Technical Report has been reviewed and is approved for publication.

Edward G. Taylor

Edward G. Taylor, Lt, USAF
Aeromechanics and Materials Division

Unclassified

SECURITY CLASSIFICATION OF THIS PAGE (When Data Entered)

REPORT DOCUMENTATION PAGE	READ INSTRUCTIONS BEFORE COMPLETING FORM
1 REPORT NUMBER: SAMSO TR-76-102	2 GOVT ACCESSION NO. / 3 RECIPIENT'S CATALOG NUMBER
4 TITLE (and Subtitle): An Investigation of Nose Bluntness Effects on Transition Asymmetry and Transition Aerodynamics,	5 TYPE OF REPORT & PERIOD COVERED: Final Report, May 1976 - September 1976
	6 PERFORMING ORG. REPORT NUMBER: 14 TRW-28513-6014-RU-00
7 AUTHOR(s): Gerald Gustafson	CONTRACT OR GRANT NUMBER(s): F04701-75-C-0163
9 PERFORMING ORGANIZATION NAME AND ADDRESS: TRW Defense and Space Systems Group, One Space Park, Redondo Beach, California 90278	10 PROGRAM ELEMENT, PROJECT, TASK AREA & WORK UNIT NUMBERS
11 CONTROLLING OFFICE NAME AND ADDRESS: Space and Missile Systems Organization, P.O. Box 92960, Worldway Postal Center, Los Angeles, California 90009	12 REPORT DATE: 30 September 1976
	13 NUMBER OF PAGES: 37
14 MONITORING AGENCY NAME & ADDRESS (if different from Controlling Office)	15 SECURITY CLASS (of this report): Unclassified
	15a DECLASSIFICATION DOWNGRADING SCHEDULE

16 DISTRIBUTION STATEMENT (of this Report)

Approved for public release; distribution unlimited.

17 DISTRIBUTION STATEMENT (of the abstract entered in Block 20, if different from Report)

18 SUPPLEMENTARY NOTES

2. Reentry bodies -- Bluntness
3. Boundary layer transition --

19 KEY WORDS (Continue on reverse side if necessary and identify by block number)

1. Boundary Layer Transition
Asymmetric Transition
Sharp Cone
Blunt Cone

20 ABSTRACT (Continue on reverse side if necessary and identify by block number)

The effects of wind fixed boundary layer transition on reentry vehicle aerodynamics plays an important role in determining high altitude trajectory dispersions. An investigation was undertaken to determine the effects of nose bluntness on boundary layer transition asymmetry and transitional aerodynamic perturbations at angle of attack. The results of previous experimental investigations of asymmetric transition are reviewed. An experimental program using the Calspan 96-inch shock tunnel to investigate bluntness effects on transition asymmetry and related aerodynamic perturbations is discussed. Data from the test

DD FORM 1 JAN 73 1473 EDITION OF 1 NOV 65 IS OBSOLETE

Unclassified

SECURITY CLASSIFICATION OF THIS PAGE (When Data Entered)

407 637

Block 20 Continued

program will be published in a future report.

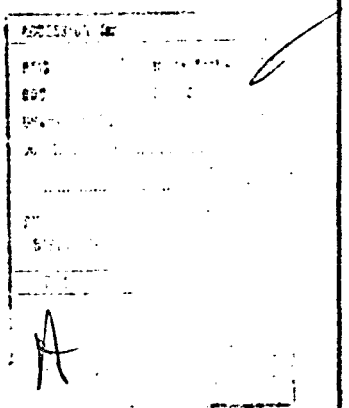

SUMMARY

The effects of wind fixed boundary layer transition on reentry vehicle aerodynamics plays an important rule in determining high altitude trajectory dispersions. An investigation was undertaken to determine the effects of nose bluntness on boundary layer transition asymmetry and transitional aerodynamic perturbations at angle of attack. The results of previous experimental investigations of asymmetric transition are reviewed. An experimental program using the Calspan 96-inch shock tunnel to investigate bluntness effects on transition asymmetry and related aerodynamic perturbations is discussed. Data from the test program will be published in a future report.

PREFACE

This final report documents the work completed by TRW under Contract Number F04701-75-C-0163 for the period from May 1976 through September 1976. The Project Officer was Captain Ed Taylor (RSSE). Mr. Dan Nowlan and Mr. Walt Portenier monitored the program for Aerospace Corporation. Particular acknowlegement is given to Dr. Michael Holden (Calspan Corporation) for his contributions to the experimental program.

TABLE OF CONTENTS

LIST OF ILLUSTRATIONS

1.0 INTRODUCTION

Reentry vehicle (RV) design problems encountered 10 to 15 years ago were largely related to ensuring the survivability of a relatively large, high yield weapon to impact. Missile guidance and control errors were the dominant contributors to the impact accuracy performance. Reentry error contributions did not place any particularly difficult constraints on the RV design.

The evaluation of performance requirements derived for future strategic weapon systems has placed significant emphasis on height of burst and impact accuracy. The improvements in several impact error sources (for example, guidance and control, geodesy, and winds and density) have resulted in a situation where the overall weapon system accuracy is now strongly influenced by impact errors produced during reentry. The prediction of reentry errors will, therefore, play a significant role in the design selection of an RV configuration and in the targeting of an operational vehicle. SAMSO/ABRES has initiated several programs intended to provide the basic technology required to develop engineering methods that analytically model accuracy related reentry performance in terms of relevant RV design parameters.

One aspect of the reentry accuracy problem is concerned with high altitude dispersions associated with boundary layer transition (BLT) from laminar to turbulent flow over the vehicle surface. An experimental and analytical program was undertaken by TRW, in conjunction with Calspan Corporation, to investigate nose bluntness effects on boundary layer transition asymmetry and transitional aerodynamic perturbations at angle of attack. This report describes the work done by TRW for the period from 1 May 1976 to 30 September 1976.

The remainder of this Section consists of background information which provided the motivation for defining the program requirements and objectives. Presented in Section 2.0 is a review of results from selected related experimental programs. The data discussed in Section 2.0 serves to illustrate the understanding of nose bluntness and angle of attack effects on boundary layer transition asymmetry prior to the start of our TRW/Calspan

investigation. Details and status of the TRW/Calspan experimental program are presented in Section 3.G.

1.1 BACKGROUND

The design evolution of operational reentry vehicles has led to relatively small, high ballistic coefficient, slender sphere-cone configurations. An impact error contribution of increasing practical interest for these vehicles has been trajectory deflections produced as the RV experiences boundary layer transition. The observation that boundary layer transition influences RV motion is not new as a review of flight test data will show that nearly all reentry vehicles exhibit some angle of attack divergence during transition (see, for example, Reference 1-3). The resulting angle of attack creates a lift force that is capable of producing a trajectory deflection whose magnitude depends on the character of the vehicle dynamic motion.

During the 1960's considerable effort was expended in analytical and ground test investigations to determine how boundary layer transition affects RV aerodynamic stability and produces the observed angle of attack divergence. The primary motivation for these efforts was established by attempts to design an endo-atmospheric decoy to match full size RV radar cross section behavior. Little, if any, substantial effort was directed towards relating BLT effects to impact accuracy degradation. Details of these investigations can be found in References 2 and 3 which are Transactions of Dynamic Stability Workshops held at AEDC in 1965 and at NASA/Ames in 1968. The early concern was the effect of so-called symmetric transition, i.e. the effect of increased frustum heating rates on an ablating body when transition moves forward of the base. Later it was shown that the effect of asymmetric transition, i.e. the skewing of the transition front due to angle of attack, on vehicle stability was possibly an even stronger effect.

Within the last few years new approaches to the analysis of RV on-board motion sensor data have been developed to determine the high altitude trajectory dispersion due to boundary layer transition. The lateral acceleration data are time integrated to characterize the trajectory dispersion in

terms of a net lateral velocity perturbation, a so-called net lateral ΔV. See, for example, References 4 and 5. Using these methods the ΔV due to BLT has been determined for a number of ABRES vehicles and MMIII operational vehicles.

The various reentry vehicles analyzed encompass a wide range of variables that may influence transition behavior, e.g. nose bluntness heat shield material, cone angle, and reentry conditions (V_e - γ_e). The variability of parameters from flight makes it very difficult to correlate the observed motion behavior with specific variables and thus draw satisfactorily unambigious conclusions concerning specific cause-effect relationships. Recognizing the potential pitfalls, however, an examination of the trajectory deflections derived from the flight motion data suggests a possible indication that ΔV is decreased as the nose bluntness ratio (r_n/R_b) is increased (Reference 5). Since nose bluntness is an obviously fundamental RV design variable, this observation naturally suggests that nose bluntness should be included as a primary parameter in an investigation of BLT effects on RV aerodynamics and accuracy.

The choice of nose bluntness as a parameter of primary interest is further justified by the results of numerous investigations which have shown nose bluntness strongly affects transition onset. A blunt nose influences the transition process in a fundamental manner through the fluid mechanics. The resulting curved bow shock wave produces a variable entropy flow along the body with local flow conditions that vary with distance along the body, e.g. varying local Reynolds number and local Mach number. The effects of nose bluntness on local flow properties (the so-called entropy swallowing process) has been analyzed, for example, by Rotta (Reference 6). The significance of nose bluntness to boundary layer transition behavior is demonstrated, for example, by Coats (Reference 7). In light of this background it is reasonable to argue that nose bluntness is probably an important parameter concerning boundary layer transition asymmetry at angle of attack. An analytical approach to correlating angle of attack and nose bluntness effects on transition asymmetry was developed by Ericsson (Reference 8).

Finally, the recent efforts to develop analytical models to predict aerodynamic effects of BLT have revealed several key aspects of the problem which lack adequate experimental data to guide the engineering analyses. The wind fixed phenomena that produce high altitude dispersion are the principal subjects of the TRW/Calspan investigation and the meaningful modeling of these effects requires knowledge of transition front asymmetry. As will be discussed in Section 2.0, there have been only 2 previous experimental programs that measured in extensive detail the axial and circumferential asymmetry of boundary layer transition at angle of attack. Furthermore, these experiments used only sharp cone models so that we have previously had no data to define the detailed effects of nose bluntness on transition asymmetry. An obvious aspect of the TRW/Calspan program was thus motivated by the desire to expand the experimental data base by measuring transition asymmetry on blunt cones.

The transitional aerodynamics analytical models incorporate the effects of wall shear increase through the transition region and the viscous-inviscid weak interaction pressure increases in order to compute aerodynamic force and moment perturbations. Since the boundary layer transition processes are so poorly understood, another motivation for the current investigation was the desire to provide additional data describing the physical mechanisms of transition that may influence the aerodynamics. Examples of these concerns are the extent of the transition region, the variation of shear and pressure through the transition region, the characteristic features the boundary layer exhibits as it goes from laminar to fully turbulent flow, etc.

2.0 REVIEW OF RELATED EXPERIMENTS

As disusssed above, the transition front asymmetry at angle of attack plays a key role in the engineering analysis of wind fixed BLT contributions to high altitude trajectory dispersion. The purpose of this Section is to present the principal results of related experimental investigations of transition asymmetry. These results illustrate the general level of understanding which existed at the beginning of the TRW/Calspan program concerning nose bluntness and angle of attack effects on transition asymmetry. Also, these data were used to guide the definition of our test objectives, model design, instrumentation requirements, and test condition matrix.

2.1 SHARP CONE SPATIAL TRANSITION MAPPING

In order to compute BLT effects on aerodynamic forces and moments it is necessary to have an adequate spatial specification of transition front asymmetry. The axial location of transition onset (and the location of fully turbulent flow) must be given as a function circumferential location around the body. A review of the literature has revealed only two experimental investigations that have measured transition asymmetry in adequate three dimensional detail (References 9 and 10). It is also important to point out that these two test programs used only essentially sharp cone models (bluntness ratio of 0 to .02). No references were found to any experiments that made similarly detailed spatial transition measurements on blunt sphere-cones.

- MOCKAPETRIS AND CHADWICK (REFERENCE 9)

An extensive investigation of transition asymmetry was performed by AVCO under Task 4.0 - Reentry Vehicle Stability - of the ABRES REST Program and the results are reported in Reference 9. Wind tunnel tests were conducted in AEDC Tunnel C at Mach 10 to obtain spatial distribution of the boundary layer transition zone on a shape 8-degree cone with ablating and non-ablating walls. To simulate an ablating surface the test model was provided with a paradichlorobenzene shell. The transition location was observed using a shadowgraph system with a 2 microsecond spark duration to provide an instantaneous picture of the state of the boundary layer. As a

second method for locating transition, as well as a means of providing data for correlation with the optical results, heat transfer data using calorimeter gages were obtained. Thirty calorimeters were used located along two meridians 180 degrees apart. In order to measure the circumferential transition asymmetry with the two meridian instrumentation a model rotation scheme was used. The boundary layer transition location was observed for 0, 36, 72 and 90 degree model rotations.

A composite picture of the BLT distribution on the non-ablating model for several angles of attack is shown in Figure 1. Shown in Figure 2 are the detailed transition asymmetry results presented in the form of transition location on the cone surface versus circumferential or meridian angle for angles of attack of 1, 2, and 3 degrees. Transition location at angle of attack is normalized by the location of transition at zero angle of attack, i.e. $X_T/X_{T_{\alpha=0}}$. It was found that the ablating model mass addition to the boundary layer caused transition to occur earlier than the non-ablating case but it did not change the general pattern of the transition asymmetry. At non-zero angle of attack the transition location on the windward surface was observed to move aft slightly with increasing angle of attack (see Figure 2). On the leeward surface, however, the transition location was observed to move rapidly forward with increasing angle of attack. The results of these tests thus show that angle of attack produced a strong transition front asymmetry on a sharp 8-degree cone. Apparently the leeward side forward transition movement is strongly influenced by the destabilizing influence of boundary layer cross-flow effects (Reference 8).

- MARTELLUCCI (REFERENCE 10)

Another extensive program to experimentally determine the effects of asymmetric transition on RV aerodynamic stability was carried out by GE and the results are reported in Reference 10. The test program to map transition and to measure the effects of asymmetric transition, with and without mass addition, was carried out in AEDC Tunnel B at Mach 8. To simulate ablating surface mass addition effects, a special porous shell force model was fabricated to allow air to be forced into the boundary layer. The spatial distribution of blowing over the model surface was controlled by using impervious sleeves over the model to block the mass addition in certain

regions. The shapes of the sleeves were made to simulate the asymmetric transition patterns measured on a separate non-blowing heat transfer model. The heat transfer model used for transition mapping was a 7.2 degree stainless steel cone. Transition location was determined from heat transfer measurements using 100 thermocouples installed along five conical rays at meridian angles of 0, 45, 90, 135, and 180 degrees. The model had a sharp nose and two spherical noses of small bluntness (r_n/R_b of .01 and .02).

A composite picture of the BLT distribution for the sharp nose model at several angles of attack is shown in Figure 3. Shown in Figure 4 are the sharp cone detailed transition asymmetry results plotted in the form of transition location on the cone surface versus meridian angle for angles of attack of 1, 2, and 4 degrees. Transition location was defined to be the end of the transition region. The data presented in Figures 3 and 4 show the transition location on the windward surface moved slightly aft with increasing angle of attack whereas the leeward surface transition location moved rapidly forward as angle of attack was increased. Comparing these results with the data of Mockapetris and Chadwick (Figures 1 and 2) shows the transition asymmetry characteristics for sharp cones, as measured by the two different techniques, to be in good general agreement.

Similar transition mapping measurements were done for the two spherical noses of bluntnesses of .01 and .02. Tests could be made only for these very small nose bluntnesses, as opposed to the larger bluntnesses of actual reentry vehicles, because of the limited ability to achieve natural transition on blunt bodies at the Tunnel B flow conditions. A composite picture of the measured transition distributions on the .02 bluntness model is shown in Figure 5 for several angles of attack. Comparison of these transition patterns with those of the sharp cone shown in Figure 3 shows that even the small increase in nose bluntness from 0 to .02 had a significant influence on the transition asymmetry pattern. This result is not suprising since investigations of nose bluntness and entropy swallowing effects on transition have shown that only very small departures in nose bluntness away from the perfectly sharp nose has a strong influence on transition onset (see, for example, Reference 6, 7, 8, 11 and 12). Thus, the need is clearly established to include realistic bluntness ratios in investigations of transition asymmetry.

The results of the force tests performed in the GE program showed the effect of mass addition was to strongly increase the magnitude of the force and moment perturbations as compared with the no blowing situation.

2.2 WINDWARD - LEEWARD TRANSITION MEASUREMENTS

As mentioned previously a search of the literature revealed only the two investigations discussed in Section 2.1 that made detailed spatial mappings of the transition asymmetry. However, there have been a number of previous investigations that determined the effects of nose bluntness and angle of attack by measuring transition location on only the windward and leeward meridians. While this limited information on transition asymmetry is not adequate to fully define the transition pattern for use in computational models, the relative movement of transition on the windward and leeward meridians does give a crude measure of the "skewness" of the transition asymmetry pattern.

Sharp cone models were used in numerous previous investigations of angle of attack effects on transition movement. Shown in Figure 6 are data from selected tests which shows transition movement on the windward and leeward meridians as a function of angle of attack. The location of transition at angle of attack (X_T) is normalized by the transition location at zero angle of attack ($X_{T\alpha=0}$) in order to clearly demonstrate the effect of angle of attack on transition movement. Data from the AVCO tests (Reference 9) and the GE tests (Reference 10) discussed in Section 2.1 are shown. Also shown are data from References 13-15. The familiar trend for sharp cones is demonstrated where transition moves slightly aft on the windward meridian and rapidly forward on the leeward meridian as angle of attack is increased. Excellent agreement is shown for these data which were taken in different facilities using different model fabrication and instrumentation techniques.

One of the earliest and most interesting investigations of nose bluntness effects on transition movement was done by Stetson and Rushton (Reference 14). These experiments were carried out in an AVCO shock tunnel at Mach 5.5. The model utilized was a 6 inch base diameter 8 degree cone with pyrex inserts containing thin platinum resistance thermometer-type heat

transfer gages. Transition location was determined from the heat transfer rates on the model surface. Transition movement with angle of attack was measured on models with a sharp nose and with spherical noses of r_n/R_b = .042 and .083.

Shown in Figure 7 are data which demonstrates the effect of nose bluntness and angle of attack on transition movement along the windward and leeward meridians. Again the transition location at angle of attack is normalized by the transition location at zero angle of attack for the particular nose. The absolute location of transition was, of course, at different distances for each of the noses employed. However, for each bluntness, the transition location at angle of attack was normalized by the location at zero angle of attack for that particular nose in order to unambiguously demonstrate the transition movement. Examination of Figure 7 shows that nose bluntness had a strong effect on transition movement with angle of attack. On the leeward meridian, the blunt cone transition location moved rapidly forward in a manner qualitatively similar to that for the sharp cone. However, as bluntness was increased, the transition location was found to move rapidly forward on the windward meridian also. This behavior is in marked contrast to the sharp cone where the windward transition location moves slightly aft with increasing angle of attack.

The relative movement of transition on the windward and leeward meridians provides a crude measure of the skewness of the transition front. The data of Stetson and Rushton indicate that increasing nose bluntness tends to decrease the skewness of the transition front. Shown in Figure 8 are the data from Reference 14 replotted in the form of X_{T_W}/X_{T_L} versus angle of attack and nose bluntness to show a measure of transition skewness. The sharp cone produces the most skewness because transition moves aft on the windward meridian and forward on the leeward. The blunt cones have less skewness because transition moved forward on both meridians, although by different amounts. These results suggest that wind-fixed transition dispersions may be reduced by use of blunt noses because the effect of increasing bluntness tends to decrease the amount of transition front skewness (asymmetry). Caution must be invoked, however, because significant circumferential asymmetries could be present that were not detected by measuring only windward-leeward transition locations.

An investigation was carried out by Muir and Trujillo (Reference 15) to repeat and extend the measurements of Stetson and Rushton. The tests were conducted in NOL Tunnel Number Eight at Mach 6. The models used were stainless steel 8 degree cones with interchangeable noses. Heat transfer measurements were made with 24 to 29 thermocouples located along the windward and leeward meridians. Transition movement with angle of attack was measured on models having nose bluntnesses r_n/R_b = .01, .08, and .32.

Shown in Figure 9 are the resulting data from Reference 15 demonstrating transition movement on the windward and leeward meridians as a function of angle of attack and nose bluntness. Data for the essentially sharp model (r_n/R_b= .01) shows the familiar transition movement characteristic of sharp cones. Data for the .08 bluntness cone showed as angle of attack increased transition moved rapidly forward on the leeward meridian and only slightly aft on the windward much in the manner observed for the sharp cone. This result is in marked contrast to the Stetson-Rushton data (Figure 7) for .08 bluntness which found transition moved rapidly forward on the windward as well as the leeward meridian. Finally, the data shown in Figure 9 for the .32 bluntness cone did indicate that transition moved forward on the windward meridian as angle of attack increased. However, for this large bluntness they observed the strange result that transition moved rapidly aft on the leeward meridian contrary to all of the observations previously discussed. Mentioned in Reference 15 are some potential difficulties in interpreting the transition data for the .32 bluntness cone because of apparent transient transition behavior related to wall cooling ratio changing during the rather long test times.

2.3 CONCLUSIONS

After reviewing the problem background and the results of related experiments in the previous Sections it remains to summarize what was concluded from this exercise. The following primary observations are listed below:

- The development of analytical transitional aerodynamics models requires detailed specification of the spatial distribution of transition over the vehicle surface.

- Nose bluntness (and the related variable entropy flow) has been demonstrated to exert a strong influence on boundary layer transition.
- Only two previous experiments made detailed spatial transition mapping measurements at angle of attack and these tests used only sharp cones or cones of very small bluntness.
- No references were found that described detailed transition asymmetry measurements for blunt cones of moderate to large bluntness ratios characteristic of actual reentry vehicles.
- Experiments which measured transition movement on only the windward and leeward meridians did consider a wide range of bluntness ratio and these data provide a crude measure of the skewness of the transition front.
- The tests of Stetson and Rushton indicated that increasing the amount of nose bluntness decreased the skewness of the transition front.
- The results of Muir and Trujillo obtained data which in some cases was contrary to the Stetson-Rushton data.

3.0 TRW/CALSPAN EXPERIMENTAL PROGRAM

An experimental program was undertaken by TRW, in conjunction with Calspan Corporation, to investigate nose bluntness effects on transition asymmetry and on the aerodynamic perturbations resulting from transition. Dr. Michael S. Holden was principal investigator for the Calspan effort which was performed under a separate AFOSR contract. TRW and Calspan jointly participated in the definition of program objectives and in the test planning. Calspan had primary responsibility for model design, fabrication, and instrumentation; for conduct of the tests, and for reduction of the raw data. TRW and Calspan will jointly participate in the data analysis and interpretation.

Subjects of investigation for the experimental program were determined from the review of related work (Section 2.0) which revealed specific gaps of knowledge or, at best, very limited information on areas of fundamental importance to the adequate modeling of high altitude dispersions due to wind-fixed transition. Also, experimental program objectives were coordinated with Dr. Hartley King of Effects Technology, Inc. who is responsible for developing the computational models of high altitude transition related trajectory dispersions.

The key issues identified to guide the TRW/Calspan experimental program were the following:

1)- How does transition front movement with angle of attack behave on sharp and blunt cones?

2) What the physical mechanisms associated with transition that produce aerodynamic perturbations?

3) What are the relative magnitude of aerodynamic perturbations due to transition on sharp and blunt cones?

4) Can the choice of nose shape and nose bluntness produce entropy swallowing effects which reduce the amount of transition asymmetry?

3.1 TEST OBJECTIVES

The primary objectives defined for the experimental program were the following:

1) Experimentally determine transition movement with angle of attack over blunt and sharp cones.

2) Identify characteristics of the transition process that may influence the aerodynamic behavior.

3) Measure the magnitude of force and moment perturbations due to transition on sharp and blunt cones.

4) Provide transition asymmetry data as a function of angle of attack, nose bluntness, and nose shape for use in flight dynamics computer models.

3.2 TEST FACILITY DESCRIPTION

The facility selected for the experimental program was the Calspan Corporation 96-inch shock tunnel. The Calspan shock tunnel was selected because of its flow simulation capability, the availability of miniaturized high frequency response instrumentation, and the ability to conduct simultaneous heat transfer, pressure, and aerodynamic force and moment measurements with a single model. The performance capability of this shock tunnel provides a wide range of Mach number and free stream unit Reynolds number combinations that are indicative of flight.

A complete detailed description of the Calspan shock tunnels is presented in Reference 16. The tunnel is started by rupturing a double diaphragm which permits high pressure gas (usually a helium-air mixture) in the driver section to expand into the driven section. A normal shock is generated and propagates through the low pressure air of the driven section. A region of high temperature, high pressure air is produced between this normal shock front and the contact surface interface between the driver and driven gas. The downstream end of the shock tube is terminated by a convergent-divergent nozzle. The ratio of the nozzle throat area to the shock tube cross-sectional area is small. Therefore, the primary normal shock wave is nearly completely reflected upstream from the throat leaving a "reservoir" region of almost stagnant, compressed, heated air at the downstream end of the dirven tube. This processed air is then expanded through the nozzle to obtain the desired hypersonic free stream conditions in the test section.

By proper control of the initial conditions in the driver and driven sections, the driver-driven gas interface becomes transparent to the shock wave reflected upstream from the throat. No gasdynamic waves result from the interface-shock interaction that could subsequently disturb the steady test air reservoir supply conditions. Since the states of the gases on

both sides of the interface must be carefully matched, this method is called the tailored interface. Under this method the test time is controlled either by the time taken for the driver-driven interface to reach the throat or the time required for the leading expansion wave (reflected from the upstream end of the driver section) to deplete the reservoir pressure behind the reflected shock. Useful testing times of 5 to 25 milliseconds can be obtained depending on incident shock Mach number and the length of the driver section.

The basic components of the 96-inch leg are shown in Figure 10. This leg consists of a chambered shock tube with an area ratio (driver/driven) of 1.56. The 5-inch inner diameter driver is 16 feet in length and can be externally heated by a resistance heater to 1260°R. The 4-inch I.D. driven tube is 48.5 feet in length. A hydrogen-nitrogen or helium-air mixture is used as the driver gas. Air is generally used as the driven gas. Four axisymmetric nozzles are available.

Nozzle	Type	Exit Diameter (inches)	Test Section Mach Number
A	Contoured	24	6.5 to 8.2
D	Contoured	48	10 to 17
E	10½° Semi-angle cone	48	7 to 22
F	10½° Semi-angle cone	72	8.6 to 24

The combined performance of the two legs covers free stream unit Reynolds number (per foot) from 10^3 to 10^8 and Mach numbers from 5.5 to 24. This Reynolds number-Mach number performance capability is shown in Figure 11.

Data acquisition is accomplished by recording transducer output on a NAVCOR magnetic drum system, on CEC and AMPEX FM tape recorders, and/or on oscilloscopes. The automatic NAVCOR system records up to 48 channels of data in digital form on a magnetic drum. Maximum available recording time is 15 milliseconds with a 50 microsecond sampling interval. The readout cycle involves transferring of the data serially from the magnetic drum to binary coded decimal tape and to a digital-analog converter. The digital voltages are transferred to magnetic tape for later reduction. At the same time these digital voltages may be transferred to a digital to analog converter at a speed compatible with a direct-writing strip chart

recorder to provide on-line monitoring of the test. Oscilloscopes may also be used to supplement the NAVCOR digital data system if it is necessary to record more that 48 channels. Data recording is accomplished by photographing the outputs of the dual-beam oscilloscopes.

3.3 MODEL DESIGN AND INSTRUMENTATION

The basic model used for the test program was a 5.725-inch base diameter 6 degree half angle cone provided with interchangeable noses. The nose configurations used consisted of a sharp tip, two spherical noses of r_n/R_b = .06 and .21, and two bluff elliptical noses (2:1 ellipse) with bluntness ratios of .06 and .21 based on the radius at the nose-frustum tangent point.

The model surface was extensively instrumented to provide detailed spacial and temporal measurements of surface heat transfer and pressure. Heat transfer measurements were made using thin film resistance thermometers. These gages are fabricated by depositing a thin platinum film on a pyrex button. The button gages are mounted in holes in the model face and set flush with the model surface. The thermal capacity of the gage is negligible. Therefore, the instantaneous surface temperature of the backing material is related to the heat transfer rate by the classical semi-infinite slab theory. Analog networks are used to convert the outputs of the gages, which are proportional to surface temperature, to a voltage which is directly proportional to heat transfer rate. Flush mounted, high frequency response pressure transducers were used to make the pressure measurements.

The model had 11 heat transfer gages located along both the windward (0°) and leeward (180°) meridians. 5 heat transfer gages were installed along each of the 90, 135, 270, and 315 degree meridians. 8 pressure gages were installed along both the 0 and 180 degree meridians.

The model was mounted on a six-component accelerometer force balance to obtain complete aerodynamic force and moment measurements simultaneously with the heat transfer and pressure measurements. Flow field photographic coverage was obtained with a spark schlieren system with a spark duration of approximately one microsecond.

3.4 TEST MATRIX

The test objectives described in Section 3.1 were used to generate a comprehensive test plan. Using heat transfer data the axial location of transition onset will be determined for each instrumented ray. The asymmetric shape of the t nsition front will be specified by processing the transition location data into the following form:

$$\frac{X_{TR}}{X_{TR_o}} = f\ (\alpha, \phi, r_n/R_b)$$

where

X_{TR} = axial transition location at angle of attack

X_{TR_o} = axial transition location at zero angle of attack

α = angle of attack

ϕ = body meridian angle

r_n/R_b = bluntness ratio

The aerodynamic effects of asymmetric transition will be determined by processing the force and moment data into the following form:

$$\Delta C_m = (C_m)_{TR} - (C_m)_{LAM}$$

$$\Delta C_N = (C_N)_{TR} - (C_N)_{LAM}$$

where

C_m = pitching moment coefficient

C_N = normal force coefficient

$( )_{TR}$ = value during transition

$( )_{LAM}$ = laminar flow value without transition

The test requirements to obtain the required data have been summarized in Table I.

The test matrix of runs made during the Calspan test program is shown in Table II.

3.5 PROGRAM STATUS

A test plan was prepared (Reference 17) and coordinated with Calspan in early May 1976. Conduct of the test program was started at Calspan on 28 July 1976 and testing was completed on 28 August 1976. Calspan is currently in the process of reducing the heat transfer, pressure, and force and moment raw data into engineering units and will be preparing data plots and tabulations. Preliminary examination of the raw data has indicated that the quality of the data obtained is excellent and it is expected that all program objectives will be met. It is expected that TRW will receive a complete set of reduced data from Calspan in mid-October.

4.0 REFERENCES

1. Sacks, I. and Schurmann, E.E.H., "Aerodynamic Phenomena Associated with Advanced Reentry Systems," AVCO RAD TM-63-79, December 1963.

2. ———— ,"Transactions of the Second Technical Workshop on Dynamic Stability Testing," Arnold Engineering Development Center, Arnold Air Force Station, Tennessee, April 20-22, 1965. (Secret)

3. Peterson, Victor L. (General Chairman),"Transactions of the Third Technical Workship on Dynamic Stability Problems," NASA Ames Research Center, Moffett Field, California, November 4-7, 1968.(Secret)

4. Blum, C. E., "Mark 12 Accuracy Improvement Final Technical Report, Phase I," TRW Report 25456-6055-TE-00, 30 June 1975. (Secret)

5. Blankenship, V. D., Patay, S. A., and Williams, T. G., "High Altitude RV Dispersion," TRW Report 28513-6006-TE-00, 1976 April (Secret); also presented at July 1976 AIAA Strategic Sciences Meeting.

6. Rotta, Nicholas R., "Effects of Nose Bluntness on the Boundary Layer Characteristics of Conical Bodies at Hypersonic Speeds, New York University Report NYU-AA-66-66, November 1966.

7. Coats, Jack D., "Investigation of the Effects of Nose Bluntness on Natural and Induced Boundary Layer Transition on Axisymmetric Bodies In Supersonic Flow," AEDC-TR-73-36, February 1973.

8. Ericsson, Lars. E., "Correlation of Attitude Effects on Slender Vehicle Transition," AIAA Journal, April 1974, pp. 523-529.

9. Mockapetris, L. J. and Chadwick, G. A., "Three-Dimensional Hypersonic Flow Boundary Layer Transition Distribution on a Sharp 8-Degree Cone With Ablating and Non-Ablating Walls at Small Angles of Attack," AVCO Report AVMSD-0599-67-CR, 25 July 1967.

10. Martellucci, A., "Asymmetric Transition Effects on the Static Stability and Motion History of a Slender Vehicle," SAMSO TR-70-141, January 1970.

11. Ericsson, L. E., "Entropy Gradient Effects on Blunted Cone Transition," AIAA Paper No. 75-195.

12. Cleary, Joseph W., "Effects of Angle of Attack and Nose Bluntness on the Hypersonic Flow Over Cones," AIAA Paper No. 66-414, June 1966.

13. McCauley, W. D., Saydah, A., and Bueche, J., "The Effect of Controlled Three Dimensional Roughness on Hypersonic Laminar Boundary Layer Transition," AIAA Paper No. 66-26, January 1966.

14. Stetson, Kenneth F. and Rushton, George H., "Shock Tunnel Investigation of Boundary Layer Transition at M = 5.5," AIAA J. May 1967.

15. Muir, James F. and Trujillo, Amado A., "Experimental Investigation of the Effects of Nose Bluntness, Free Stream Unit Reynolds Number, and Angle of Attack on Cone Boundary Layer Transition at a Mach Number of 6," AIAA Paper No. 72-216, January 1972.

16. ——— , "Calspan Hypersonic Shock Tunnel, Description and Capabilities Brochure," 1973.

17. Gustafson, G. Q. and Deffenbaugh, F. D., "An Experimental Plan to Investigate Nose Bluntness Effects on Boundary Layer Transition Asymmetry and Aerodynamic Perturbations at Angle of Attack," TRW Report, March 1976.

TABLE I

TEST REQUIREMENTS

NOSE SHAPE	$\frac{r_n}{R_b}$	α	OBJECTIVES
Sharp	0	2°	Laminar flow, no transition. These runs provide the baseline inviscid force and moment data.
Sphere	.06	2°	
Sphere	.21	2°	
Bluff	.06	2°	
Bluff	.21	2°	
Sharp	0	0	Obtain asymmetric transition shape, force, and moment data on a sharp cone (without entropy swallowing).
Sharp	0	1	
Sharp	0	2	
Sharp	0	3	
Sphere	.06	0	Determine the effects of spherical bluntness on transition asymmetry, forces, and moments.
Sphere	.06	1	
Sphere	.06	2	
Sphere	.06	3	
Sphere	.21	0	
Sphere	.21	1	
Sphere	.21	2	
Sphere	.21	3	
Bluff	.06	0	Determine effects of nose shape on transition asymmetry, forces and moments. Also, the bluff nose should produce a stronger entropy swallowing effect than the spherical nose.
Bluff	.06	1	
Bluff	.06	2	
Bluff	.06	3	
Bluff	.21	0	
Bluff	.21	1	
Bluff	.21	2	
Bluff	.21	3	

TABLE II

CALSPAN TEST RUN MATRIX

CALSPAN RUN NO.	NOSE SHAPE	$\frac{r_n}{R_b}$	α	M_∞	$R_{e\infty}$ 10^6/FT.
2	Sharp	0	0	13.04	4.761
3	Sharp	0	0	12.97	4.714
4	Sphere	.06	0	12.96	4.579
5	Sphere	.06	3°10'	13.00	4.973
6	Sharp	0	0°7'	13.30	3.100
7	Sharp	0	1°4'	13.35	3.042
8	Sharp	0	0°7'	12.72	2.967
9	Sharp	0	0°9'	12.43	1.792
10	Sphere	.06	3°6'	12.60	2.208
11	Sphere	.06	2°10'	13.00	4.894
12	Sphere	.06	3°7'	12.44	1.689
13	Sphere	.06	1°7'	13.01	4.732
21	Sphere	.21	3°3'	11.35	10.31
25	Sphere	.21	2°12'	11.36	10.25
27	Sphere	.21	3°10'	11.01	3.960
28	Sphere	.21	2°10'	11.00	3.829
43	Sharp	0	3°7'	13.54	2.840
44	Sharp	0	3°7'	13.00	1.082
45	Sharp	0	2°9'	13.54	2.711
46	Sharp	0	2°9'	12.96	1.132
47	Sharp	0	2°9'	13.40	1.665
48	Sharp	0	3°7'	14.80	1.573
49	Sphere	.06	0°7'	11.34	10.67
50	Ellipse	.06	0°9'	11.32	9.812
51	Sphere	.06	3°12'	11.33	9.666
52	Sphere	.06	1°8'	11.49	10.33
53	Sphere	.06	1°8'	10.96	3.158
54	Ellipse	.21	1°8'	11.35	9.950
55	Sphere	.06	0°37'	11.33	10.53
56	Ellipse	.06	3°7'	11.34	10.17

TABLE II

CALSPAN TEST RUN MATRIX

(Continued)

CALSPAN RUN NO.	NOSE SHAPE	$\frac{r_n}{R_b}$	α	M_∞	$R_{e\infty}$ 10^6/FT.
57	Ellipse	.06	3°7'	10.89	2.395
58	Sphere	.21	0°9'	8.70	12.85
59	Sphere	.21	0°7'	8.79	22.97
60	Sphere	.21	0°7'	8.82	38.73
61	Sphere	.21	0°7'	8.55	5.418
62	Sphere	.21	1°9'	8.54	5.252
63	Sphere	.21	3°7'	8.54	5.242
64	Sphere	.21	2°9'	8.56	5.357
65	Sphere	.21	2°9'	8.63	7.874
66	Ellipse	.21	2°9'	8.61	8.053
67	Sphere	.21	3°7'	8.62	8.129
68	Sphere	.06	3°7'	8.56	5.534
69	Sphere	.06	0°7'	8.54	5.300

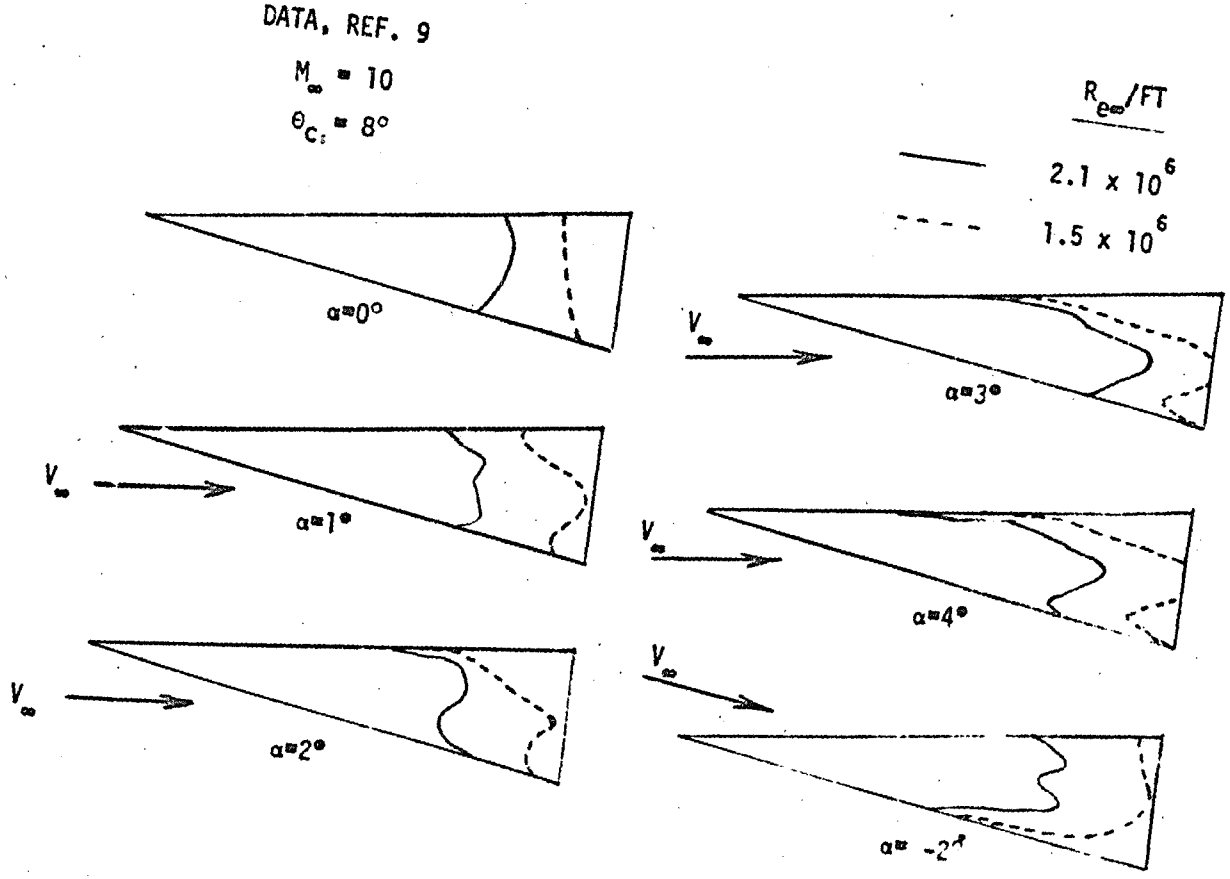

Figure 1. Composite transition distribution, sharp cone, (Mockapetris and Chadwick, Reference 9)

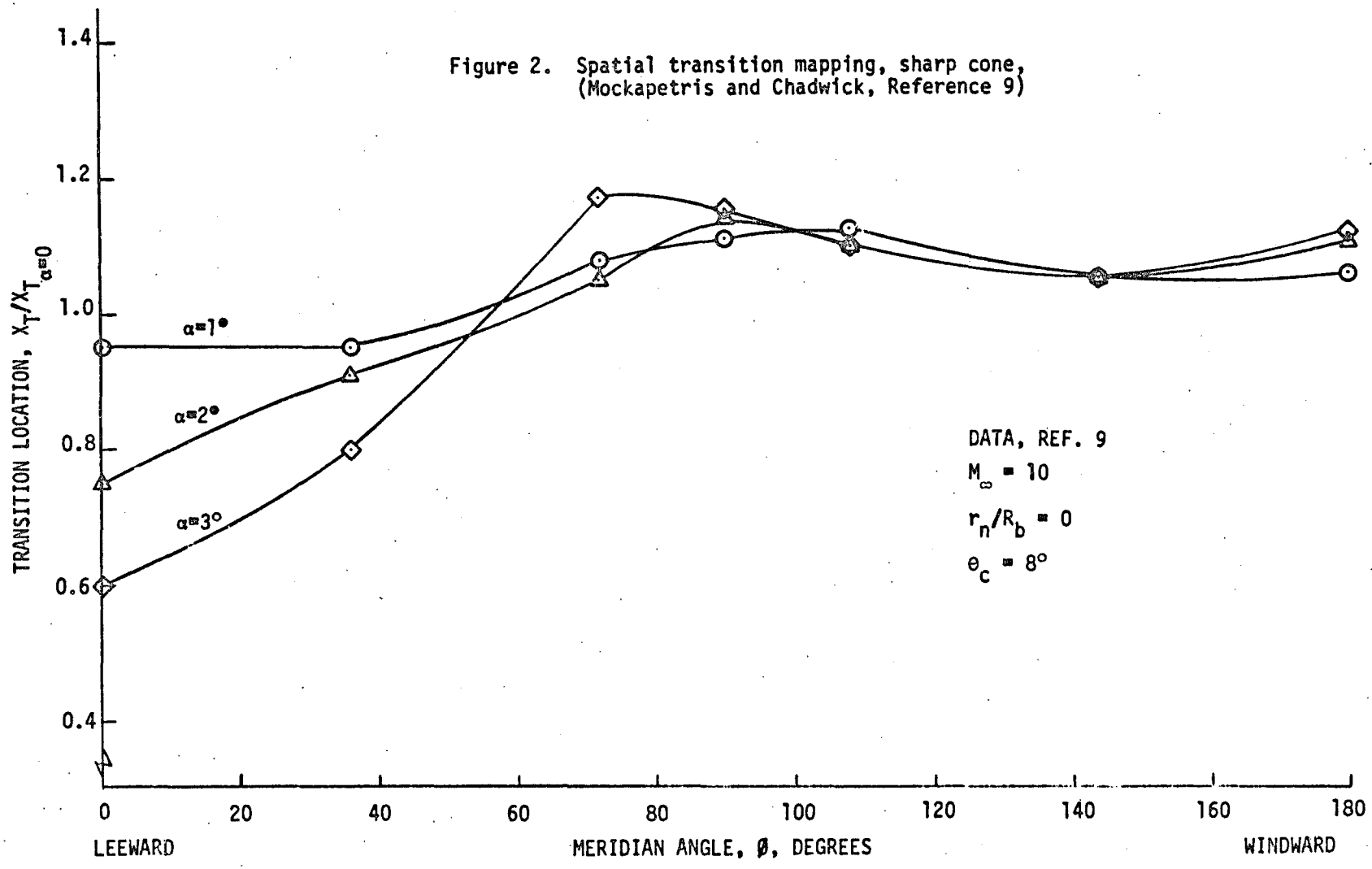

Figure 2. Spatial transition mapping, sharp cone, (Mockapetris and Chadwick, Reference 9)

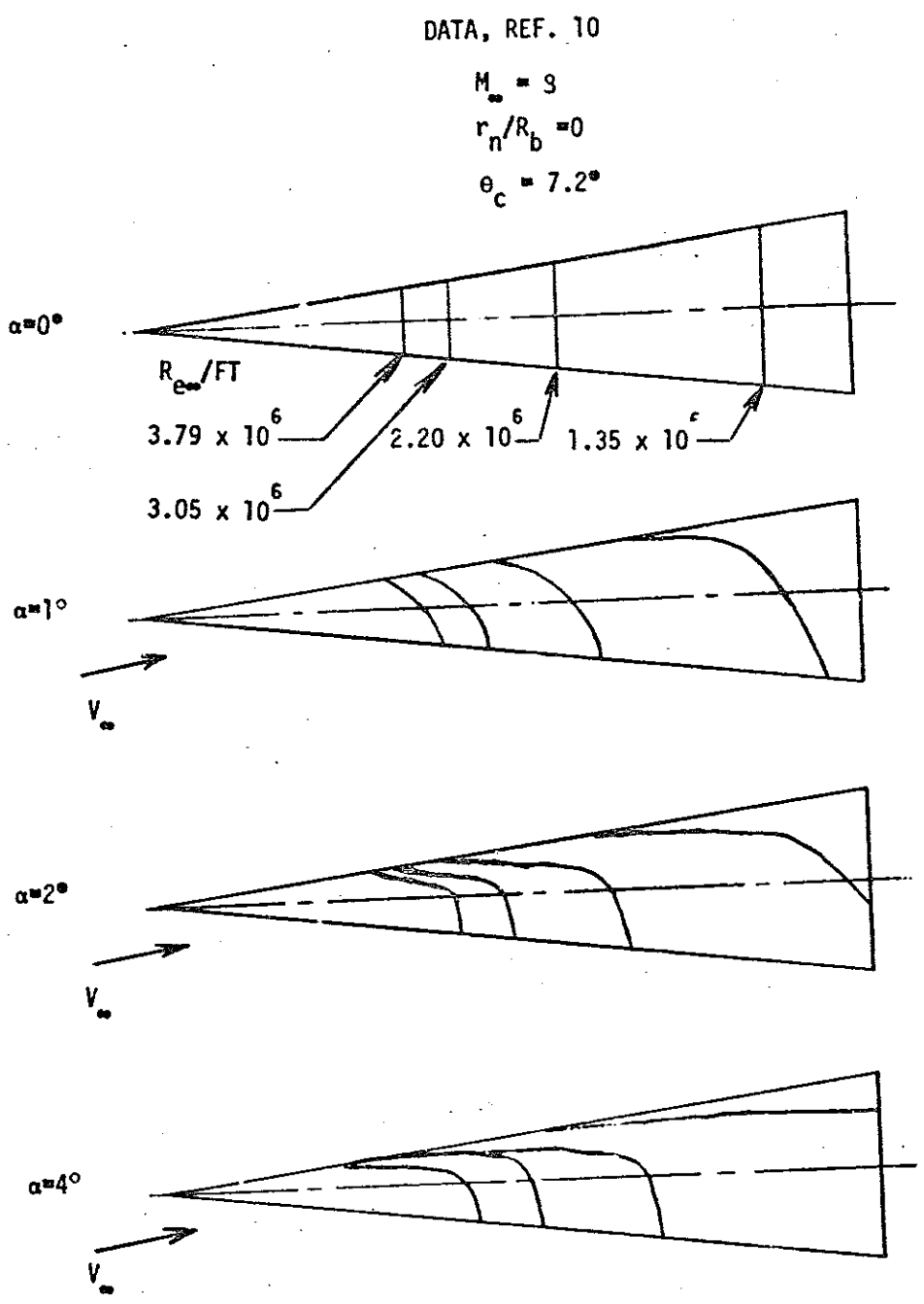

Figure 3. Composite transition distribution, sharp cone, (Martellucci, Reference 10)

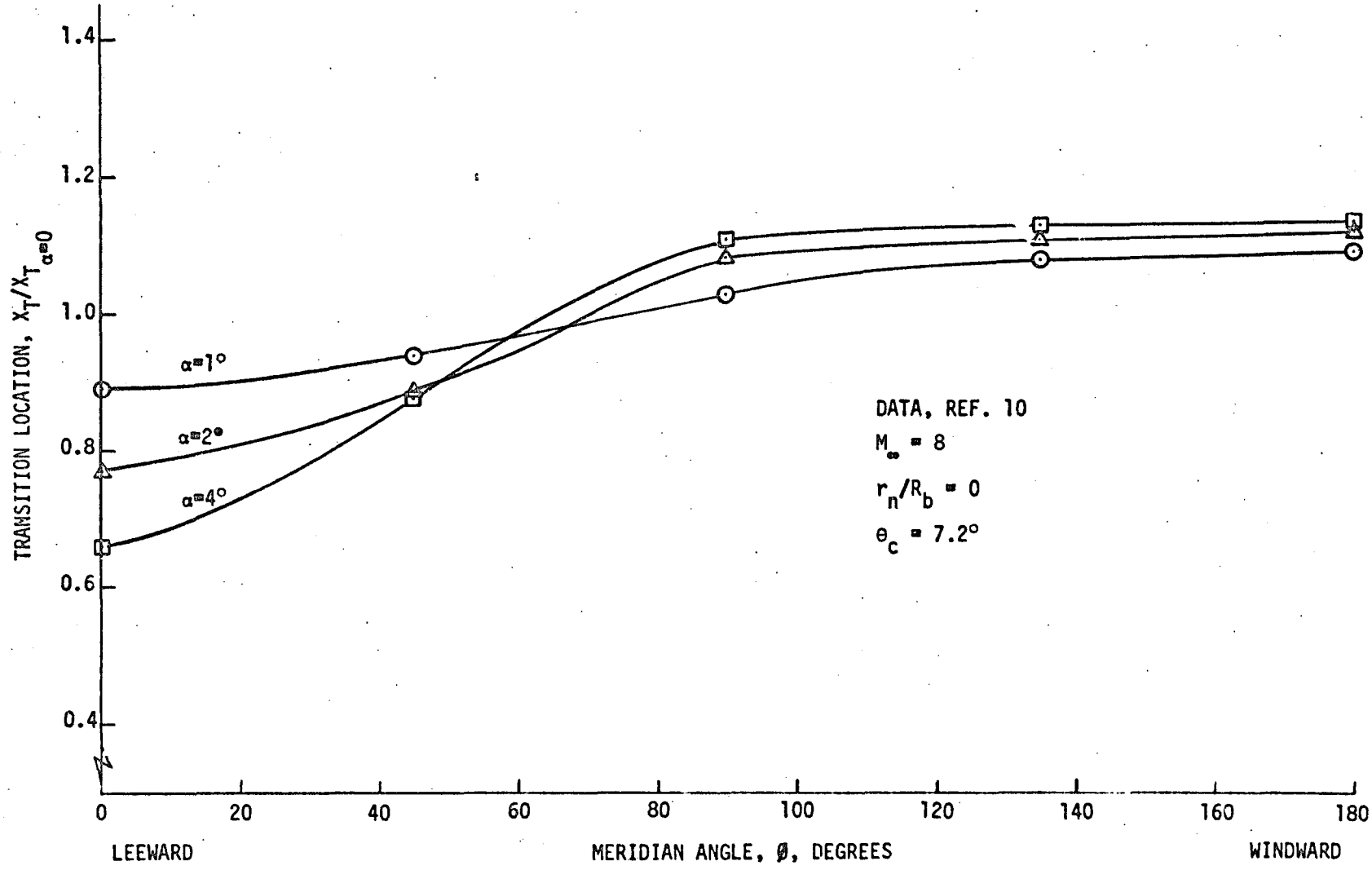

Figure 4. Spatial transition mapping, sharp cone, (Martellucci, Reference 10)

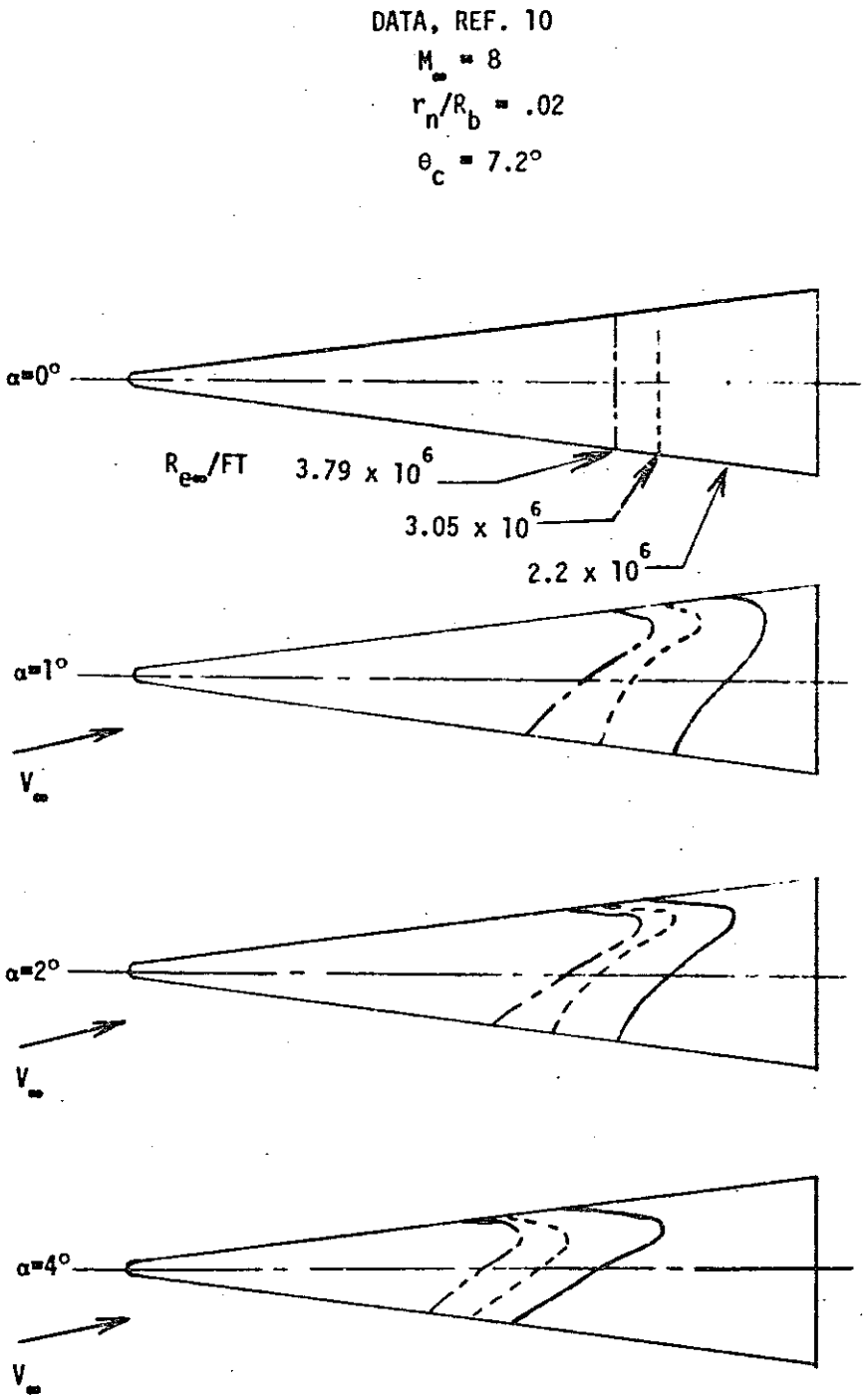

Figure 5. Composite transition distribution, r_n/R_b = .02, (Martellucci, Reference 10)

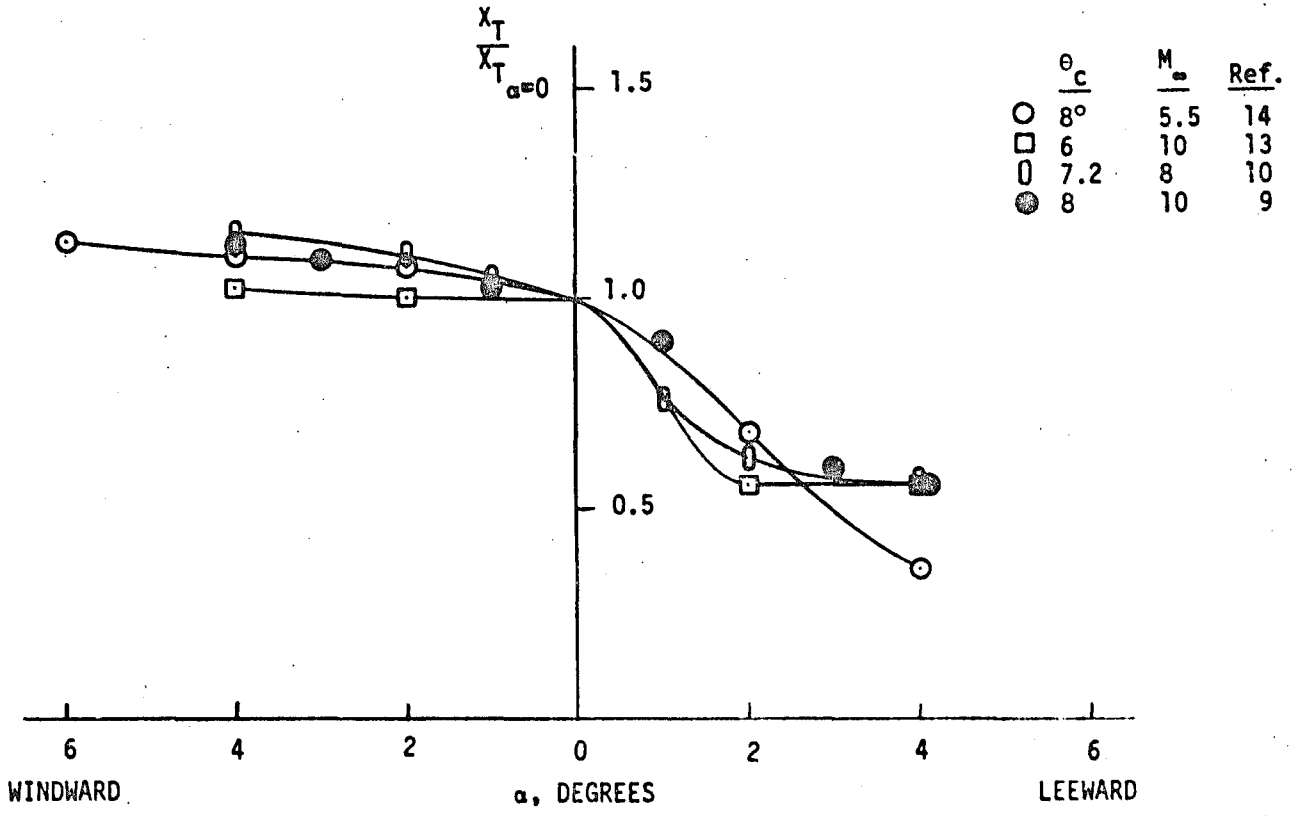

Figure 6. Windward-leeward transition movement, sharp cone

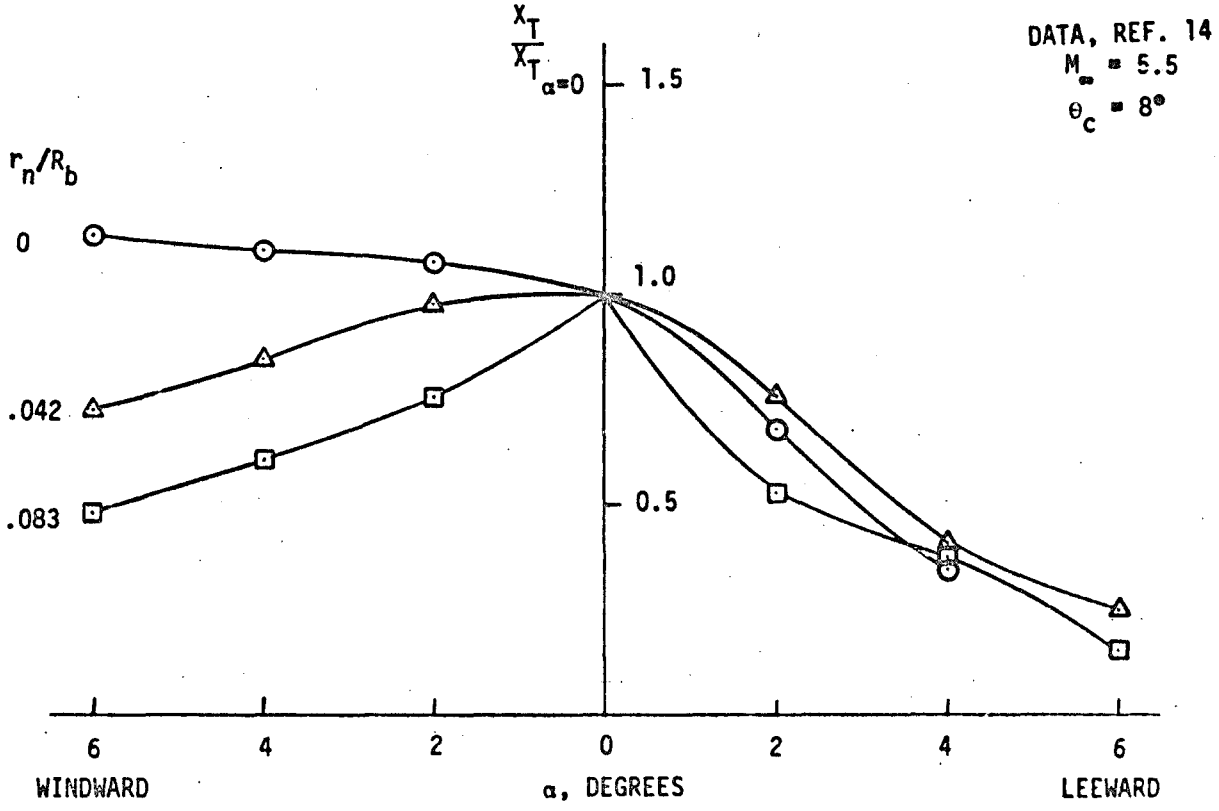

Figure 7. Windward-leeward transition movement, sharp and blunt cones, (Stetson and Rushton, Reference 14)

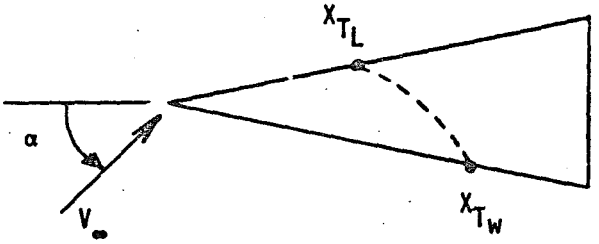

DATA, REF. 14
M_∞ = 5.5
θ_c = 8°

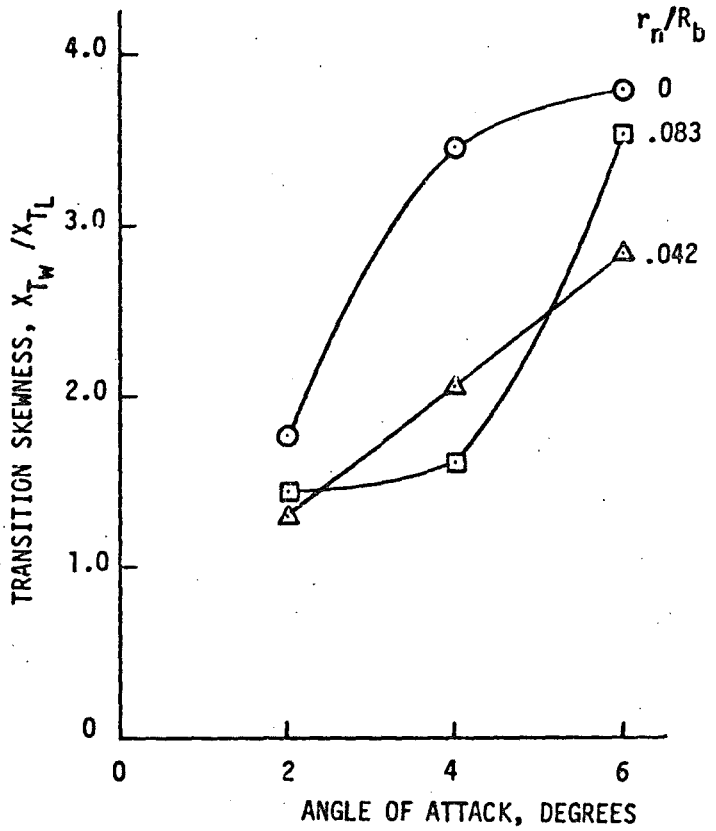

Figure 8. Bluntness effect on transition skewness, (Stetson and Rushton, Reference 14)

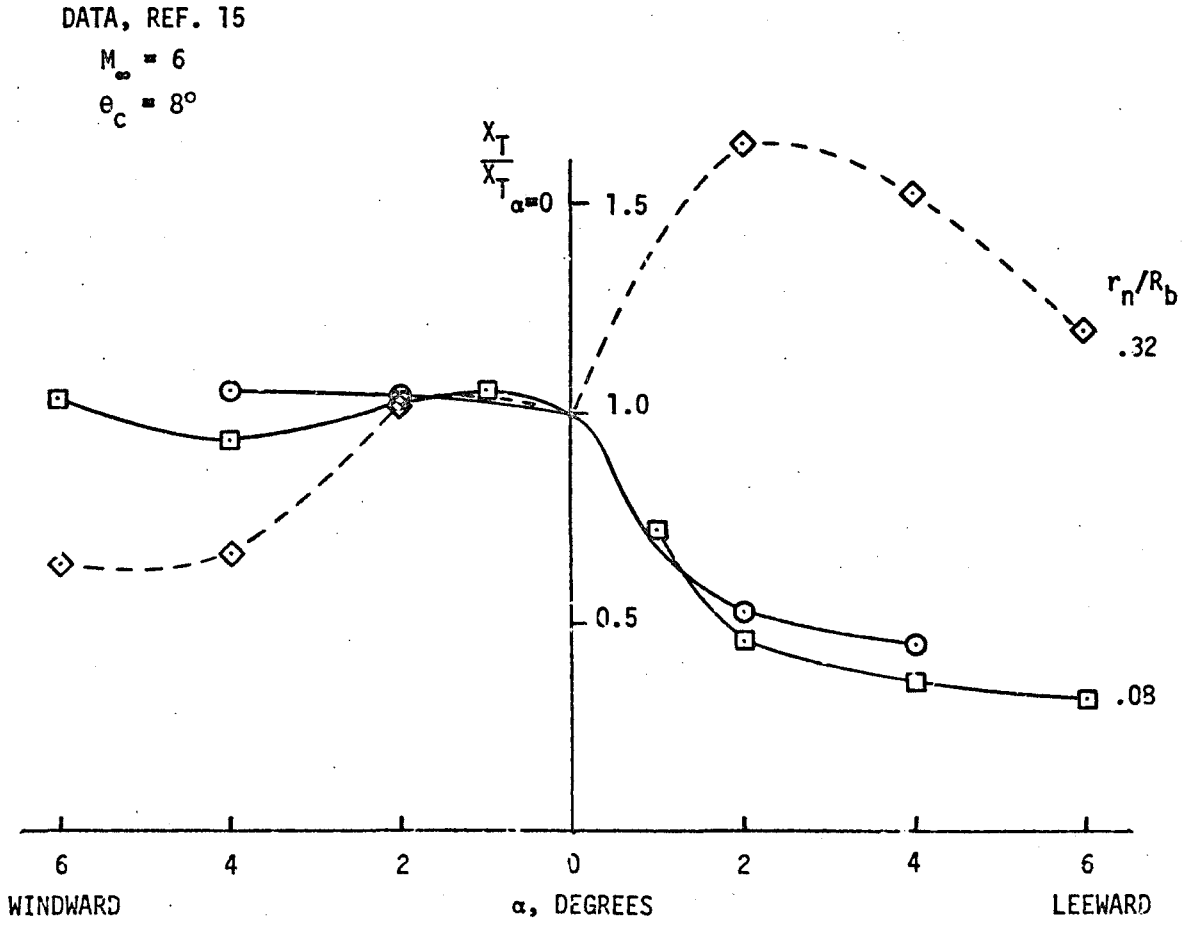

Figure 9. Windward-leeward transition movement, sharp and blunt cones, (Muir and Trujillo, Reference 15)

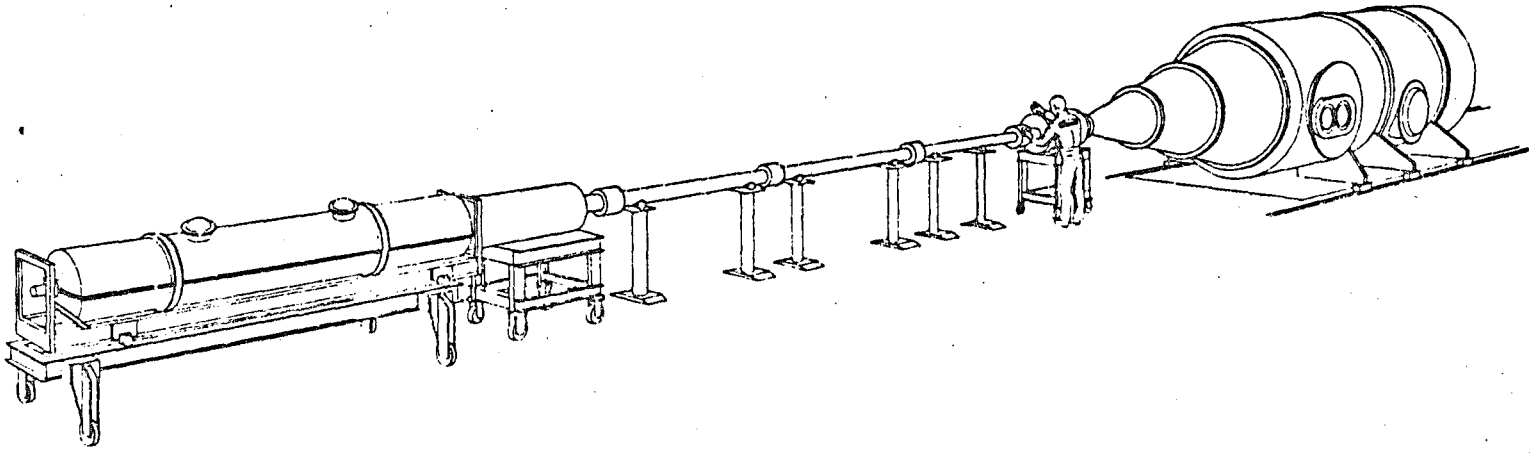

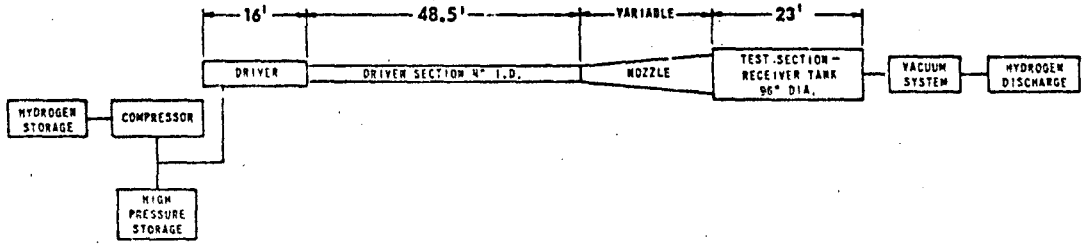

3416

Figure 10. Basic Components of the Calspan Hypersonic Shock Tunnel 96" High Energy Leg

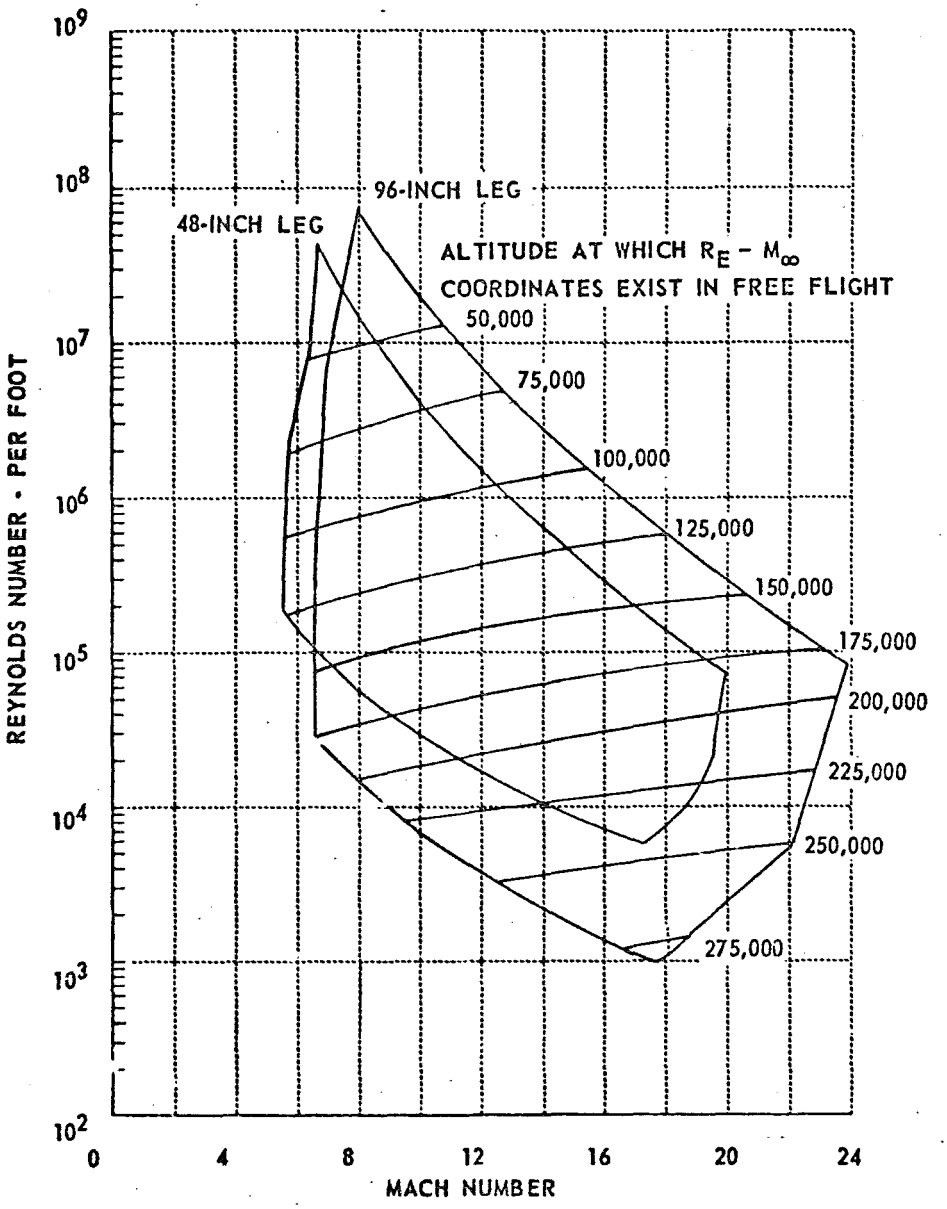

Figure 11. Calspan Hypersonic Shock Tunnel Performance

Re_{max} Based on $T_{\infty\ min} = 1.10\ T_{LOX}$